Annealing-Induced High Impact Toughness of Polypropylene/CaCO₃ Nanocomposites

Yong Lin,[1] Haibin Chen,[2] Chi-Ming Chan,[1,3] Jingshen Wu[2]

[1]Department of Chemical and Biomolecular Engineering, The Hong Kong University of Science and Technology, Clear Water Bay, Hong Kong
[2]Department of Mechanical Engineering, The Hong Kong University of Science and Technology, Clear Water Bay, Hong Kong
[3]Division of Environment, The Hong Kong University of Science and Technology, Clear Water Bay, Hong Kong

ABSTRACT: Our previous study (Macromolecule 2008, 41, 9204–9213) reported that annealing significantly increased the impact toughness of polypropylene (PP)/calcium carbonate (CaCO₃) nanocomposites. We further investigated the underlying mechanism and report the results in this article. The impact strength of a high-molecular-weight PP filled with 20 wt % CaCO₃ nanoparticles increased to 890 J/m upon 155°C-annealing, about 20 times that of neat unannealed PP. This exceptionally high impact toughness is partially attributed to the high-molecular-weight PP, which provided strong ligaments. Moreover, this high-molecular-weight PP has a low concentration of cross-hatched structure upon annealing, indicating that the cross-hatched structure, which was suspected to be responsible for the annealing-induced high impact toughness in the previous study, is in fact irrelevant to the annealing-promoted impact toughness. A large number of cavities were observed in the impact-fractured annealed nanocomposites because the difference in the stiffness between the crystalline and amorphous regions was enlarged upon annealing. These cavities, formed in the early stage of deformation, may have contributed to the annealing-induced high impact toughness because these numerous cavities, in addition to the debonding of the CaCO₃ nanoparticles, further released the plastic constraint of the PP matrix. Massive plastic deformation, therefore, became operative, leading to large energy dissipation. In addition, we found that the tensile toughness of the annealed nanocomposites was considerably reduced due to a significant reduction in the strain-at-break because the numerous cavities caused an earlier development of macro-cracks, leading to smaller strain-at-breaks. © 2011 Wiley Periodicals, Inc. J Appl Polym Sci 124: 77–86, 2012

Key words: polypropylene; nanocomposites; impact resistance; annealing

INTRODUCTION

The effects of annealing on the mechanical properties of polypropylene (PP) have been a subject of interest in the past two decades.[1–8] Increased toughness of PP upon annealing was generally observed,[1–6] though the improvement was marginal. Our previous study reported a fivefold increase in the impact toughness of PP/CaCO₃ nanocomposites on annealing at 155°C.[9] We found that the concentration of the cross-hatched structure and the impact toughness changed in a similar pattern as a function of annealing temperature. They increased as the annealing temperature increased from 150 to 155°C and then decreased when the annealing temperature further increased to 160°C. The cross-hatched structure was suspected to be one of the factors responsible for the increased impact toughness of the annealed nanocomposites.[9] The objective of this study was to determine the exact mechanism for the annealing-induced high impact toughness of PP/CaCO₃ nanocomposites.

Annealing changes the crystallographic morphology of PP, which strongly influences its mechanical properties. The correlation between morphology, such as lamellar thickness, spherulitic size as well as crystallinity, and the fracture toughness was systematically investigated by Avella et al.[10] The critical strain-energy-release rate (G_c) evaluated from Charpy impact tests increased with lamellar thickness and varied according to the degree of super-cooling. However, as the authors pointed out, the effects of each individual parameter on fracture toughness are difficult to explicitly delineate because the crystallinity, spherulitic size, and lamellar thickness cannot be changed independently and there is interplay among these parameters. Annealing of PP at high temperatures usually involves partial-melting and re-crystallization due to the enhanced mobility of the polymer chains. Micro-morphological

changes usually include: (1) perfection of existing crystals; (2) thickening of lamellae; and (3) newly formed crystals.[11–15] Based on the three distinct relaxation times determined by nuclear magnetic resonance (NMR) measurements,[12,16] the microstructure of PP can be classified into three regions, which are assigned to be (1) the rigid regions, referring to the crystalline domains; (2) the semirigid regions, referring to the interphases between the crystalline domains and the amorphous layers; and (3) the soft regions, referring to the amorphous layers. It was reported that annealing reduced the fraction of the amorphous phase, maintained the fraction of the semirigid phase, and increased the fraction of the crystalline phase.[12] The relaxation times of polymer chain segments measured by NMR serve as good indicators of the chain mobility, which is significant for mechanical responses of the polymers due to their distinguished viscoelastic properties. However, conclusions made about the change in the chain mobility in the amorphous region of PP after annealing are contradictory in two independent studies.[12,17] The chain mobility in the amorphous region was reported to increase as a result of a better organized morphology during annealing.[12] However, in another study, the chain mobility in the amorphous region was shown to decrease, which was attributed to the reduced chain lengths between the adjacent crystals.[17] Compared with the amorphous phases, the crystalline phases play a more dominant role in determining the degree of plastic deformation because the yield stress, which characterizes the resistance to plastic deformation, is proportional to the lamellar thickness and less affected by the amorphous regions.[18] Consequently, annealing is expected to impose a negative effect on the toughness of semicrystalline polymers because the increased lamellar thickness raises the resistance of polymers to plastic deformation.

However, an increase in toughness after annealing was generally observed. To understand the improved toughness upon annealing and to establish a relationship between the improved toughness and the corresponding changes in the micro-morphology, three different fracture mechanisms have been employed to characterize the fracture behavior of annealed PP. The first applied fracture mechanism is the linear elastic fracture mechanism (LEFM). Annealing of the already solidified PP samples increased G_c and the critical stress intensity factor (K_c).[1] In light of the well-accepted conclusion that the strength of interspherulitic regions is critical in determining the fracture toughness, as evidenced by the fact that the crack path preferentially goes through spherulitic boundaries if the spherulites are large and coarse,[19] Greco and Ragosta proposed that the fracture process is essentially controlled by the

interconnections within the materials and that annealing produces a more physically connected morphology through the partial-melting and re-crystallization process, leading to improved toughness.[1] When significant plastic deformation occurs in the crack front, such as in a semiductile and/or ductile fracture mode, the J-integral R-curve is applied because LEFM is no longer valid. The J-integral evaluates the fracture toughness of annealed PP at the crack-initiation stage in terms of the critical fracture initiation parameter (J_c).[2] Again, the idea of a more interconnected morphology resulting from annealing is adopted to explain the increased J_c after annealing. Frontini and Fave extended that idea by pointing out that noncrystallized components aggregating at spherulitic boundaries undergo a re-crystallization process upon annealing, leading to a more interconnected physical network to impede the craze coalescence and hence improve the fracture toughness.[2] The essential work of fracture (EWF) procedure, which separates the fracture toughness into two terms, the plastic work (ω_p) and the essential work (ω_e), can be applied to study the fracture toughness from the perspective of the micro-structure.[20,21] This method was employed by several authors to examine the fracture behavior of annealed PP. However, the results of EWF studies were controversial. Ferrer-Balas et al. showed that annealing of PP produced an increase in ω_p but a decrease in ω_e.[22] Contradictory results reported by Na and Lv indicated that both ω_p and ω_e were essentially unchanged.[23] A large number of cavities were detected by Na and Lv in the annealed PP films.[23] They proposed that these cavities have two counter-interacting effects on toughness. The deterioration of the solid fraction and the release of the plastic constraint, which cancel each other out, result in no changes in the toughness of PP after annealing. In spite of these results, the positive effect of annealing on the toughness of PP has been generally observed. However, a generally acceptable interpretation of the improved toughness upon annealing is still lacking. In this study, we further investigated the effects of annealing on the tensile and impact toughness of PP/CaCO$_3$ nanocomposites. A toughening mechanism of annealed PP/CaCO$_3$ nanocomposites is proposed based on new findings about the fracture morphology of PP/CaCO$_3$ nanocomposites. The results of this work help to resolve some of controversial issues on the annealing effects on toughness.

EXPERIMENTAL

Materials

Two kinds of isotactic PPs were used in this study. One was HJ730L (H-PP) from Samsung Company

TABLE I
Physical Properties of H-PP and E-PP

	MFI (g/10 min)	$\overline{M}_w$ (g/mol)	$\overline{M}_n$ (g/mol)	Isotacticity[c]
H-PP	5[a]	346,000	55,000	95.4%
E-PP	0.5[b]	472,000	88,000	94.8%

[a] Measured according to ASTM D1238.
[b] Measured according to JIS 7210-1999.
[c] The isotactic pentad fraction (mm%) determined using an NMR.
All data were provided by the PP suppliers.
MFI = melt flow index, $\overline{M}_w$ = weight-average molecular weight and $\overline{M}_n$ = number-average molecular weight.

and the other was EA9 (E-PP) from Japan Polypropylene. The physical properties of the PPs are listed in Table I. Calcium carbonate nanoparticles, with a trade name of SPT, were provided by Solvay Chemicals and had a surface coating of 2.3 wt % stearic acid. The diameter of these nanoparticles was about 70 nm. Stearic acid was purchased from Sigma with a 95% purity grade. An antioxidant, Irganox 1010 (0.5 wt %), was added to the PP during compounding.

Preparation of PP/CaCO$_3$ nanocomposites

The as-received CaCO$_3$ nanoparticles were treated with 4 wt % stearic acid to produce a monolayer coating on the surface. The surface coating of the nanoparticles with stearic acid was conducted in an ethanol solution at 80°C for 2 h. The coating amount needed for a monolayer was determined to be 5.3 wt % using a thermogravimetric analyzer. The detailed procedures and the characterization for the monolayer coating were reported in a previous article.[9] These monolayer-coated nanoparticles at a concentration of 20 wt % were melt-blended with H-PP or E-PP in a Haake mixer at 180°C for 15 min. The two nanocomposites were named E-5-20 and H-5-20, corresponding to the nanocomposites containing E-PP and H-PP, respectively. The detailed compounding procedures can be found elsewhere.[24]

Material characterization

The crystallization characteristics of the PPs and nanocomposites were studied using a Perkin–Elmer (Diamond 7) differential scanning calorimeter (DSC). The crystallinity was measured at the first heating scan of the injection-molded impact bars. The heat of fusion of the PP crystals was taken to be 209 J/g.[25] The micro-morphology of the nanocomposites was examined by transmission electron microscopy (TEM). Thin sections ($\sim$ 80 nm) of nanocomposites were cut using a Leica Ultract R microtome equipped

with a diamond knife at room temperature. To reveal the lamellar structures, the nanocomposites were stained with RuO$_4$. The detailed procedures of the ultramicrotomy and staining can be found in a paper by Li and Cheung[26] TEM micrographs were obtained using a JOEL 100CX II TEM operated at an accelerating voltage of 100 kV.

Mechanical tests

The injection molding conditions of the tensile and impact bars were described previously.[24] Injection-molded tensile and impact bars were annealed in an oven at 155°C for 3 h. After annealing, the samples were cooled in ambient air and conditioned at (23 ± 3)°C at a relative humidity of 50% for 24 h. The tensile tests were performed on an Instron tester using a cross-head speed of 5 mm/min in accordance with ASTM-D658. The notched Izod impact tests were conducted according to ASTM-D256. V-shaped notches were cut using a CSI automatic notcher (CS-93M). The cutter speed and the table feed rate were about 92 and 100 mm/min, respectively. The impact and tensile data were averaged on five specimens tested.

Fractographic examination

The fracture surface and the cross-section underneath the fracture surface, as schematically shown in Figure 1, were observed using a scanning electron microscope (SEM) JOEL JSM-6700F. Cryofracture was used to expose the cross-section of the impact-fractured sample. After immersing the impact-fractured sample in liquid nitrogen for more than 20 min, it was cleaved by a wedge within 3 s after the sample had been removed from the liquid nitrogen. The interior micro-morphology of the tensile-fractured bars was
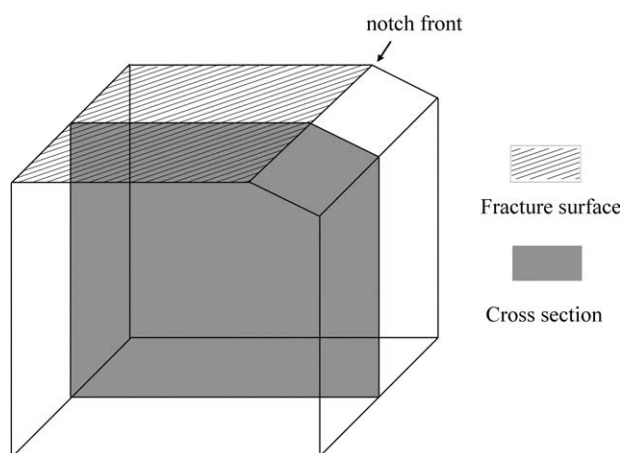

Figure 1 A schematic picture showing the fracture surface and the cross-section of an impact-fractured sample of PP/CaCO$_3$ nanocomposite for SEM observations.[9]
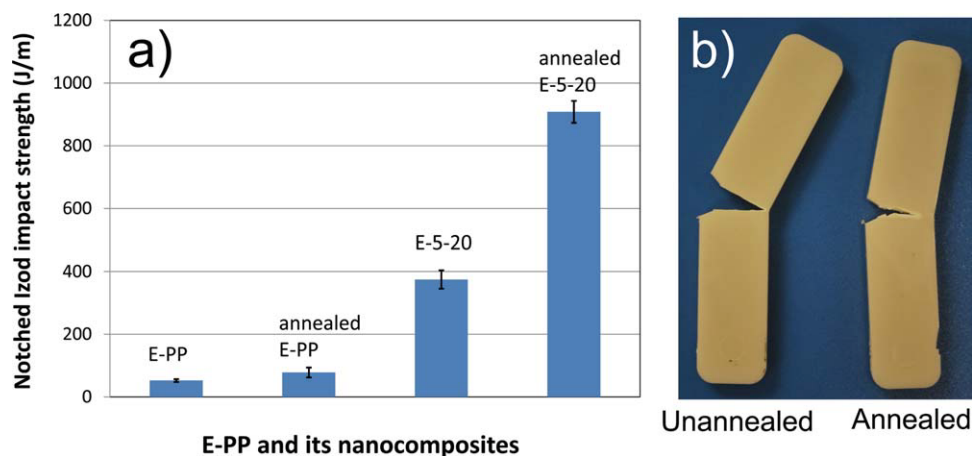
Figure 2 (a) Notched Izod impact strength of unannealed and annealed E-PP and E-5-20 samples and (b) a picture of impact-fractured bars of unannealed and annealed E-5-20 samples. [Color figure can be viewed in the online issue, which is available at wileyonlinelibrary.com.]

observed using an SEM. The examined planes parallel to the longitudinal direction of tensile bars were freshly exposed by the same cryofracture method. The SEM specimens were coated with gold; the operating voltage was 5 kV.

RESULTS AND DISCUSSION

Correlation between cross-hatched structure and the annealing-improved impact toughness

The effect of annealing on the impact strength of E-PP/CaCO$_3$ nanocomposites is clearly displayed in Figure 2(a). The impact strength of E-PP increased only moderately upon annealing. In contrast, the impact strength of unannealed E-5-20 was 370 J/m, which was considerably higher than that of unannealed E-PP because of the synergetic effect of the high-molecular-weight matrix and the well-dispersed nanoparticles.[27] Annealing substantially increased the impact strength of E-5-20 to 890 J/m, which is the highest value of impact strength of PP/CaCO$_3$ nanocomposites ever reported in the literature. The impact bars of the annealed E-5-20 were so ductile that they were only partially broken after the impact test, as shown in Figure 2(b). In addition, shear whitening was noticeable in the crack tip of the annealed sample, indicating the occurrence of intensive shear deformation.

In our previous study,[9] we found that annealing has a significant effect on the impact toughness and that the degree of the cross-hatched structure and the impact toughness changed in the same manner, first increasing with the annealing temperature from 150 to 155°C and then decreasing at 160°C. The cross-hatched structure was suspected to be the key to the improved impact strength. However, this hypothesis was overturned in this study. The

concentration of the cross-hatched structure was shown to vary with the isotacticity and the molecular weight of PP.[28,29] Compared with H-PP, E-PP has a much lower concentration of the cross-hatched structure after annealing at 155°C, as demonstrated by the DSC and TEM results (c.f., Figs. 3 and 4). An endothermic shoulder, which appeared in the DSC curve of H-5-20 after annealing, was indicative of an increased concentration of the cross-hatched structure.[9] In contrast, no distinct endothermic shoulder was detected in the DSC curve of E-5-20 after annealing as shown in Figure 3, implying that the cross-hatched structure was probably absent. This conclusion was further confirmed by a comparison between the TEM micrographs of unannealed and annealed E-5-20 samples. As shown in Figure 4, stacking lamellae overwhelmingly prevailed, but few
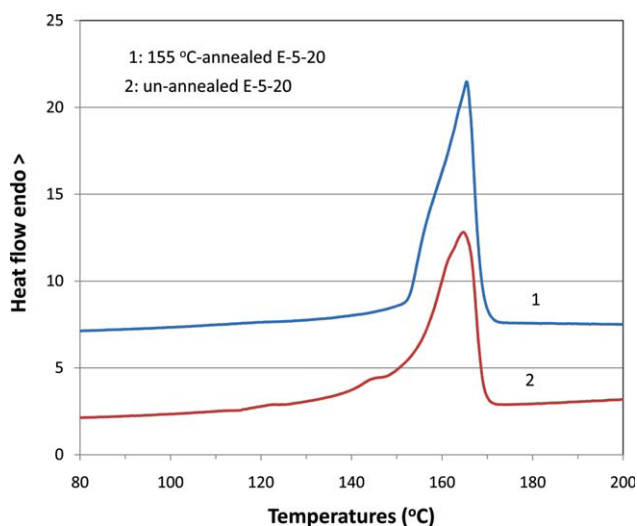

Figure 3 DSC curves of unannealed and annealed E-5-20 samples. [Color figure can be viewed in the online issue, which is available at wileyonlinelibrary.com.]
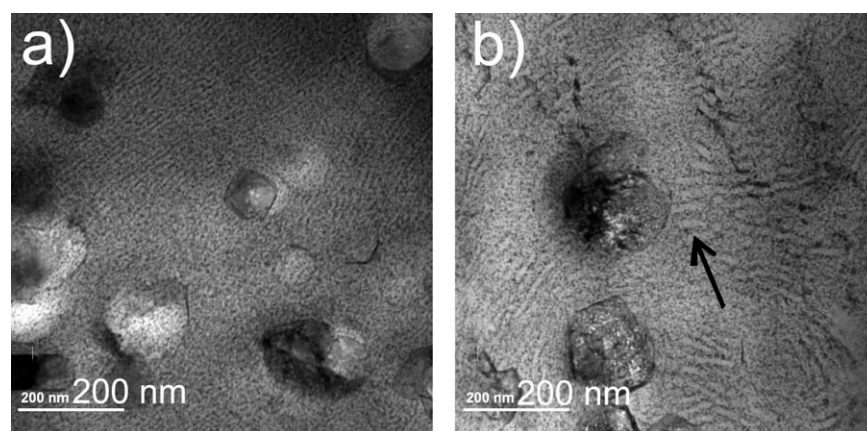
Figure 4 TEM micrographs of (a) unannealed and (b) annealed E-5-20 samples.

cross-hatched structures could be found in the annealed E-5-20 sample. In addition, the lamellar thickness of the annealed sample was noticeably larger, which is consistent with the increase in the crystallinity of the sample from 33.5 to 41.5% after annealing. The fact that the annealed E-5-20 sample has a lower concentration of the cross-hatched structure than the unannealed one but an exceptionally high impact strength demonstrates that the cross-hatched structure is not essential for the high impact strength of PP/CaCO$_3$ nanocomposites.

The micro-morphology of an impact-fractured annealed H-5-20 sample was investigated to determine whether or not the cross-hatched structure plays any role in the plastic deformation. In the TEM observations, a staining technique was employed to enhance the contrast between the crystalline and amorphous domains. The staining agent (RuO$_4$) penetrated preferentially in the amorphous phases but did not go into the crystalline phases, producing white crystalline and black amorphous regions in the TEM micrographs. In the vicinity of the notched root of an impact-fractured annealed H-5-20 sample, we found that there were some large gray areas, whose color was close to that of the crystalline domains. We believe that these large gray areas are the highly-deformed regions composed of strained polymer chains, which are aligned with a certain degree of order, limiting the deposition of RuO$_4$. Figure 5(a,b) shows the coexistence of the stacking lamellae and the cross-hatched structure under different magnifications. Both the lamellae and the cross-hatched structure were deformed and fragmented. Figure 5(c,d) displays the fragmented cross-hatched structure at low and high magnifications, respectively. The cross-hatched structure does not appear to resist the plastic deformation because they deformed as much as the stacking lamellae did.

One of the interesting findings in the TEM observations is the empty oval cavities surrounded by a white thick boundary, as shown in Figure 6(a). These empty oval cavities were originally occupied by the nanoparticles and later deformed to become oval-shaped. In addition, a white tail, which resembles a comet, was found at the polar region of an empty oval hole, as indicated by an arrow in Figure 6(b). The white boundary and the white tail can be interpreted as the localized deformation, which was intensified due to the stress concentration effect around the nanoparticles. These observations provide evidence of the crucial function played by the nanoparticles, i.e., the debonding of the nanoparticles triggers the massive plastic deformation.

Fractographic study on the annealed nanocomposites

SEM micrographs of the impact-fractured surface of an annealed E-5-20 sample are presented in Figure 7. A ripple-like morphology was observed near the notch root, as shown in Figure 7(a). Occasionally, a ductile fracture feature like fiber-tearing, as shown in Figure 7(b), was observed. Additionally, intrinsic cavities of the PP matrix were identified, as indicated by a small arrow in Figure 7(b). It should be emphasized that these tiny cavities were not a result of the debonding of nanoparticles, judging from their extremely small sizes. CaCO$_3$ nanoparticles seem to be well embedded in the fracture surface, whereas intensive plastic deformation cannot be seen. It is possible that the adiabatic heat generated during the intensive plastic deformation melted the fracture surface, leading to the encapsulation of the nanoparticles by the PP matrix again during the partial-melting and re-crystallization process.

The intensive plastic deformation was well conserved in the interior of the impact-fractured samples and can be viewed in the cross-section underneath the impact-fractured surface. The schematic picture showing the location of the cross-section is
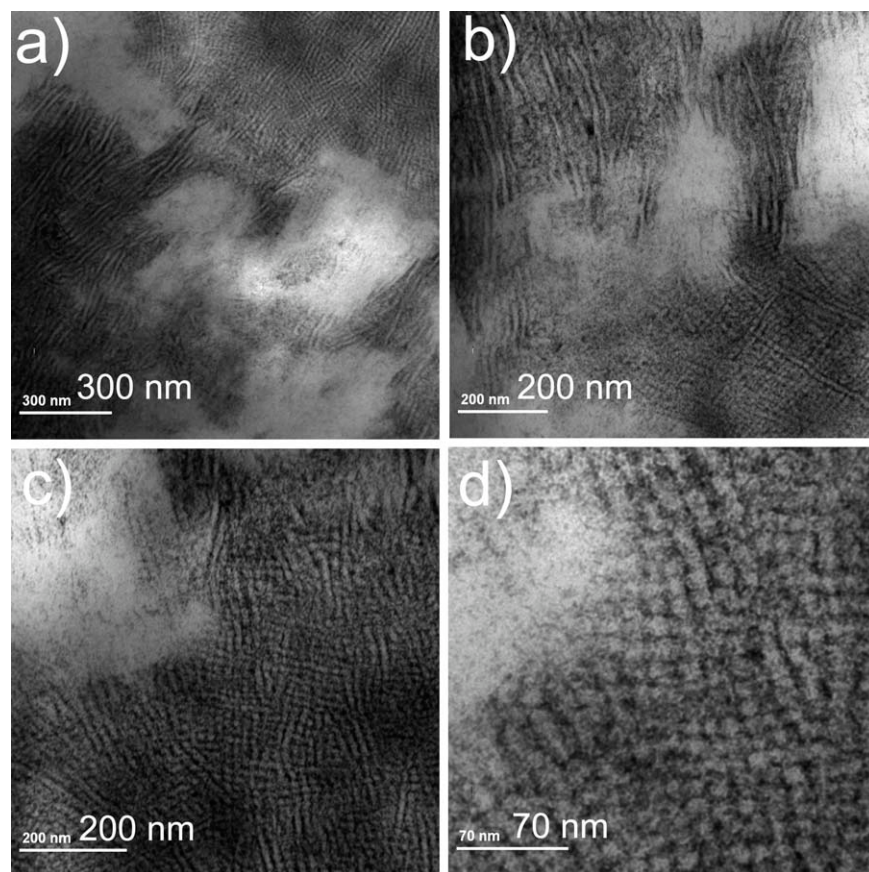
Figure 5 A series of TEM micrographs of an impact-fractured annealed H-5-20 sample in the vicinity of the notched root. Both the stacking lamellae and the cross-hatched structure deformed during the impact process.

displayed in the left corner of Figure 8. The global view and detailed structure of the plastic zone are presented in Figure 8(a,b), respectively. Intensive plastic deformation was visible in a large area. In addition, numerous cavities were present, as indicated by an arrow in Figure 8(b). The cavities were found not only in the highly-deformed region but also in the slightly-deformed region. Figure 8(c,d) was taken from an area around 500 μm beneath the fracture surface. Cavities formed in the surroundings of the nanoparticle clusters [c.f., Fig. 8(d)]. It is likely that due to the stress concentration effect, debonding and cavitation took place around the nanoparticles in sequence. The presence of the cavities in the moderately deformed area indicated that the cavitation occurred before the intensive plastic deformation,
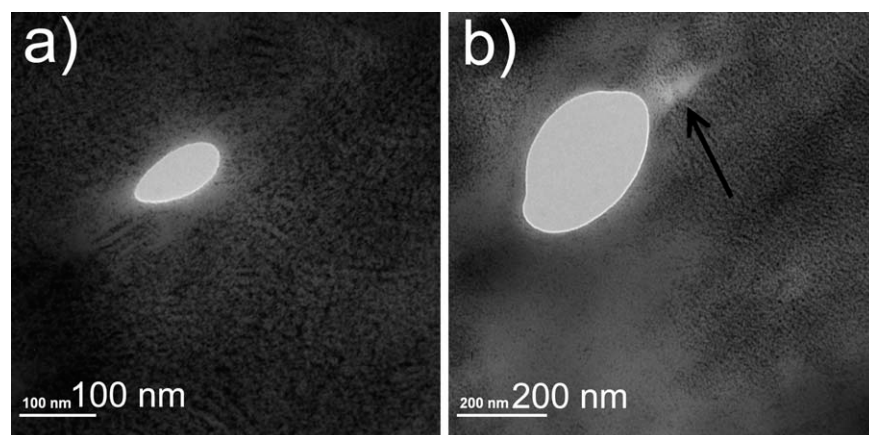

Figure 6 (a) An oval cavity surrounded by a relatively white boundary and (b) an oval cavity with a white tail at its polar region resembling a comet.
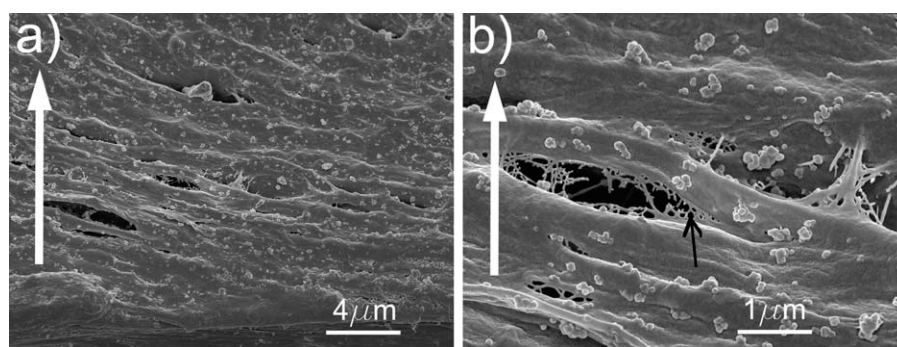
Figure 7 SEM micrograph of the impact-fractured surface of an annealed E-5-20 sample at low (a) and high (b) magnifications.

instead of resulting from it. The formation of cavities is believed to be helpful for releasing the plastic constraint of the PP matrix and responsible for the annealing-induced high impact toughness of the nanocomposites.

Influence of annealing on the tensile properties of PP/CaCO$_3$ nanocomposites

Table II summarizes the tensile-test data as well as the degree of crystallinity of E-PP and E-5-20 before and after annealing. With the addition of CaCO$_3$ nanoparticles to E-PP, the Young's modulus increased while the yield stress decreased, which is consistent with many reported results.[24,30,31] Owing

to the increased crystallinity after annealing, the Young's moduli of E-PP and E-5-20 increased. However, the slight decrease in the yield stresses of annealed E-PP and E-5-20 is unusual. The strain-at-break decreased nearly by half after annealing. Apparently, annealing caused a significant loss in the ductility of E-PP. The representative engineering stress–stain curves of unannealed and annealed E-5-20 samples are shown in Figure 9. The curve of the annealed E-5-20 sample was shifted to the right by 0.5 units for clarity. The deformation of the annealed E-5-20 sample was macroscopically homogeneous and the stress was continuously increased after yielding until fracture. In contrast, the unannealed E-5-20 sample went through a typical necking and
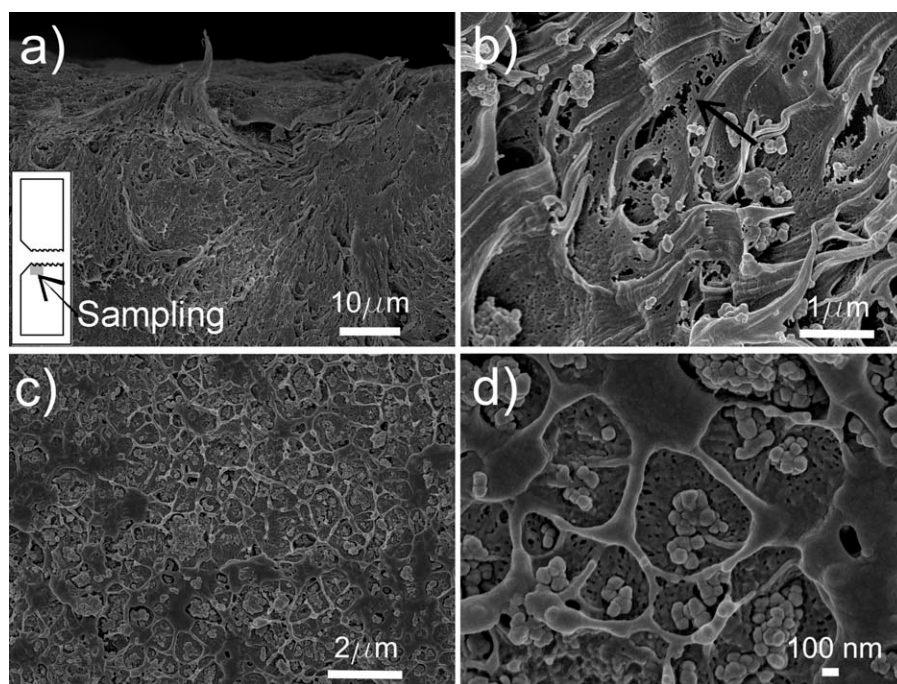

Figure 8 SEM micrographs of the cross-section of broken Izod 155°C-annealed E-5-20 samples. (a) and (b) reveal the intensive plastic deformation underneath the fracture surface. (c) and (d) were taken at locations 500 μm beneath the fracture surface. Numerous cavities can be observed in both the highly- and moderately-deformed regions. The crack-propagation direction was from left to right.

TABLE II
Tensile-Test Data and Crystallinity of E-PP and E-5-20 Before and After Annealing

Sample	Young's modulus (GPa)	Yield stress (MPa)	Strain-at-break	Stress-at-break (MPa)	Crystallinity (wt %)
U-E-PP[a]	2.53 ± 0.22	39.68 ± 1.12	6.8	45.69 ± 1.66	32.7
A-E-PP[a]	3.29 ± 0.14	38.38 ± 0.63	3.8	49.67 ± 2.09	39.7
U-E-5-20	2.98 ± 0.27	36.29 ± 0.57	6.9	41.56 ± 0.89	33.5
A-E-5-20	4.16 ± 0.16	36.04 ± 0.37	4.0	45.34 ± 0.27	41.5

[a] The prefix "U" represents unannealed and the prefix "A" represents annealed.

strain hardening process. The micro-morphologies of tensile-fractured unannealed and annealed E-5-20 samples were examined by SEM on a freshly cryo-exposed surface parallel to the longitudinal direction of the tensile bar. The SEM micrographs are presented in Figure 10. The tensile direction is horizontal, as indicated by a double-headed arrow. Complete or partial oval holes with the long axis parallel to the tensile direction were observed in the examined area of the unannealed E-5-20 sample, as shown in Figure 10(a). A close view of the oval cavities revealed that they have fine structures of fibrillated ligaments, which were generated as a result of the coalescence of cavities, as indicated by a small arrow in Figure 10(b). The general feature of the annealed E-5-20 sample is the stepwise layers, as shown in Figure 10(c). Numerous cavities were found in the connecting area of the two successive layers, as indicated by the small arrow in Figure 10(d). This implies that the slitting of two successive layers is likely due to the coalescence of numerous cavities. These cavities are probably accountable for the decrease in the yield stress and the strain-at-break after annealing. The coalescence of numerous cavities is likely to cause the development of macro-cracks at the early stage of plastic deformation, leading to the significant reduction in the strain-at-break. The cavities create stress concentrations and release the lateral constraints of plastic deformation, which probably result in the lower stress level needed for yielding.

It is interesting to notice that the effects of annealing on the toughness of E-5-20 are opposite at the low and high strain rates. The tensile toughness, which is measured by the area under the stress–strain curve, is considerably impaired after annealing due to the significant reduction in the strain-at-break, as seen in Figure 9. Conversely, the increase in the impact toughness of E-5-20 upon annealing is prominent. Elmajdoubi and Vu-Khanh reported that the fracture toughness of PP increased with crystallinity at high loading rates and decreased with crystallinity at low loading rates.[32] They suggested that the blunting effect at the crack tip due to the adiabatic heating was more significant under high loading rates. In this study, we found that numerous cavities appeared in the annealed

E-5-20 sample after deformation, which may be the source of the counter-interacting effects of the annealing found at the low and high strain rates.

Discussion on the influences of cavitation on toughness

Moderate enhancement of the PP toughness due to annealing has been generally observed. Greco and Ragosta[1] and Frontini and Fave[2] proposed that the development of a more physically interconnected network after annealing, which impedes the development of a craze, is the mechanism. In this study, a large increase in the impact toughness and a considerable decrease in the tensile toughness of $PP/CaCO_3$ nanocomposites were observed. We hypothesize that the large number of cavities is likely to be the reason for the opposite effects of annealing on toughness displayed at the low and high strain rates.

Cavitation during the plastic deformation is generally observed in semicrystalline polymers.[33] The occurrence of cavitation can be revealed by TEM observations with the OsO_4 staining technique[34] and is associated with chain scission, which usually happens in between the adjacent stacks of lamellae due to the mechanical mismatch between the crystalline and amorphous phases.[33] Annealing can increase the
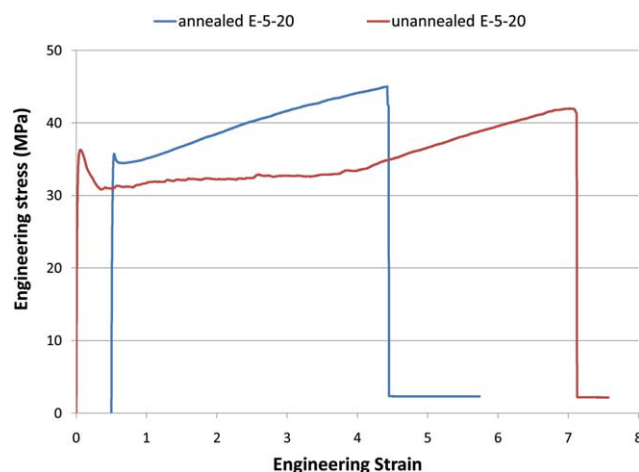

Figure 9 Representative engineering stress–strain curves of unannealed and annealed E-5-20 samples. [Color figure can be viewed in the online issue, which is available at wileyonlinelibrary.com.]
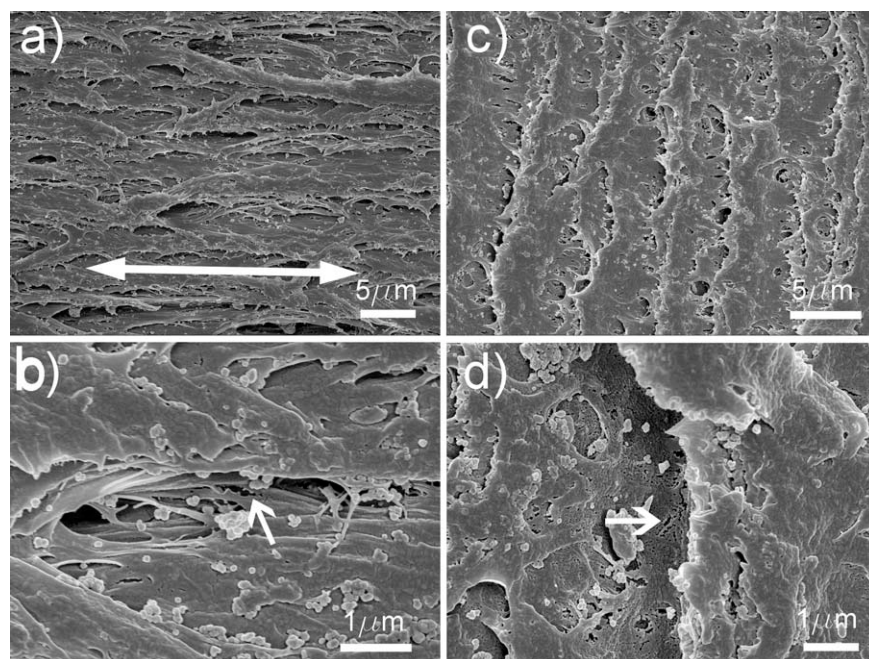
Figure 10 SEM micrographs of tensile-fractured samples, taken from freshly cryo-exposed surfaces parallel to the longitudinal direction of tensile bars. The double-headed arrow indicates the tensile direction. (a) and (b) are the unannealed E-5-20 sample, at different magnifications; (c) and (d) are the annealed E-5-20 sample at different magnifications.

number of cavities appearing during deformation, as shown in the study of annealed poly(vinylidene fluoride) (PVDF).[35]

Pawlak and Galeski performed detailed studies on the cavitation of PP using small-angle X-ray scattering.[36,37] Several important conclusions were drawn from their studies: (1) cavitation occurs just before the yield point in tensile tests; (2) PP prepared by quenching, with less perfect crystals, is able to deform by plastic deformation without cavitation during low-speed tensile tests; and (3) at high drawing rates, the cavitation in the amorphous phases is preferred due to the stronger response of the crystals. Annealing at 155°C definitely increases the lamellar thickness in our case. The number of cavities, therefore, increases significantly in the tensile-fractured and impact-fractured samples of the annealed nanocomposites. Cavities, if present in a large number, are detrimental to tensile toughness, because, at low strain rates, PP chains are able to undergo plastic deformation even without the assistance of cavitation to release the plastic constraint. The presence of cavitation in annealed E-5-20 actually leads to an early formation of numerous micro-cracks, which eventually develop into macro-cracks causing a remarkable loss in ductility. As a result, the tensile toughness, which is greatly dependent on the strain-at-break, deteriorates upon annealing. The situation is different when the strain rate is substantially higher and the plastic constraint is much more severe.

The appearance of numerous cavities is believed to play a similar but rather substantial role to the debonding of the nanoparticles, which is important for releasing the plastic constraint.[30,38–40] Cavities, formed at the early stage of deformation, are crucial and necessary for the release of the plastic constraint in addition to the debonding of the nanoparticles. As shown in another study,[41] there was a sharp brittle-to-ductile transition (BDT) as the nanoparticle concentration increased. The BDT occurred when the thickness of the ligaments was thin enough, due to a decrease of the interparticle distance, for the transition from the plane-strain to plane-stress state to take place. The formation of numerous cavities is analogous to debonding of nanoparticles to achieve thin ligaments. Admittedly, unannealed nanocomposites still have a few cavities but it is the large number of cavities in the annealed samples that makes a dramatic difference to the extent of plastic deformation and thus the ultimate impact toughness. The idea that cavities are beneficial for impact toughness of semicrystalline polymers is shared by Ravi and Takahashi.[42] As shown in their studies, the Charpy impact toughness of neat high density polyethylene increased after annealing. They proposed that annealing should increase the number of "microvoids" per unit volume, which promotes the formation of fibrillar structure, leading to the ductile deformation and the consumption of much higher fracture energy.[42] Therefore, the creation of numerous cavities is likely responsible for the massive plastic deformation of the nanocomposites upon annealing.

CONCLUSIONS

We investigated the effects of annealing on the toughness of PP/CaCO$_3$ nanocomposites in this study. The combination of high-molecular-weight PP, well-dispersed CaCO$_3$ nanoparticles, and annealing treatment produced PP/CaCO$_3$ nanocomposites with exceptionally high impact toughness of 890 J/m. The annealing-induced high impact toughness was attributed to the numerous cavities formed in the early stage of deformation, leading to the sufficient release of the plastic constraint of the PP matrix besides the debonding of the nanoparticles and hence facilitating the massive plastic deformation. The higher concentration of cavities in the deformed annealed-nanocomposites was probably caused by the stronger response of crystals to plastic deformation after annealing, as suggested by the study of Pawlak and Galeski.[36,37] On the other hand, a large number of cavities are detrimental to the tensile toughness because of the early coalescence of cavities, causing a significant loss in ductility. In summary, the effects of annealing on the toughness of PP/CaCO$_3$ nanocomposites are opposite at the low and high strain rates.

References

1. Greco, R.; Ragosta, G. J Mater Sci 1988, 23, 4171.
2. Frontini, P. M.; Fave, A. J Mater Sci 1995, 30, 2446.
3. Alberola, N.; Fugier, M.; Petit, D.; Fillon, B. J Mater Sci 1995, 30, 860.
4. Ibhadon, A. O. J Appl Polym Sci 1998, 69, 2657.
5. Seguela, R.; Staniek, E.; Escaig, B.; Fillon, B. J Appl Polym Sci 1999, 71, 1873.
6. Kitao, K.; Turuta, H. Kobunshi Ronbunshu 1995, 52, 497.
7. Drozdov, A. D.; Christiansen, J. D. Polymer 2002, 43, 4745.
8. Drozdov, A. D.; Christiansen, J. D. Polym Eng Sci 2003, 43, 946.
9. Lin, Y.; Chen, H. B.; Chan, C. M.; Wu, J. S. Macromolecules 2008, 41, 9204.
10. Avella, M.; dell'Erba, R.; Martuscelli, E.; Ragosta, G. Polymer 1993, 34, 2951.
11. Martorana, A.; Piccarolo, S.; Sapoundjieva, D. Macromol Chem Phys 1999, 200, 531.
12. Hedesiu, C.; Demco, D. E.; Kleppinger, R.; Vanden Poel, G.; Gijsbers, W.; Blümich, B.; Remerie, K.; Litvinov, V. M. Macromolecules 2007, 40, 3977.
13. Zia, Q.; Androsch, R.; Radusch, H.-J.; Piccarolo, S. Polymer 2006, 47, 8163.
14. Poussin, L.; Bertin, Y. A.; Parisot, J.; Brassy, C. Polymer 1998, 39, 4261.
15. Vittoria, V. J Macromol Sci Phys 1989, 28, 489.
16. Weglarz, W. P.; Peemoeller, H.; Rudin, A. J Polym Sci Part B: Polym Phys 2000, 38, 2487.
17. Litvinov, V. M.; Soliman, M. Polymer 2005, 46, 3077.
18. Schrauwen, B. A. G.; Janssen, R. P. M.; Govaert, L. E.; Meijer, H. E. H. Macromolecules 2004, 37, 6069.
19. Friedrich, K. Prog Colloid Polym Sci 1978, 64, 103.
20. Wu, J.; Mai, Y.-W. Polym Eng Sci 1996, 36, 2275.
21. Chen, H.; Wu, J. Macromolecules 2007, 40, 4322.
22. Ferrer-Balas, D.; Maspoch, M. L.; Martinez, A. B.; Santana, O. O. Polymer 2001, 42, 1697.
23. Na, B.; Lv, R. J Appl Polym Sci 2007, 105, 3274.
24. Chan, C. M.; Wu, J. S.; Li, J. X.; Cheung, Y. K. Polymer 2002, 43, 2981.
25. Clark, E. J.; Hoffman, J. D. Macromolecules 1984, 17, 878.
26. Li, J. X.; Cheung, W. L. J J Appl Polym Sci 1999, 72, 1529.
27. Lin, Y.; Chen, H. B.; Chan C. M.; Wu, J. S. Polymer 2010, 51, 3277.
28. Janimak, J. J.; Cheng Z. D.; Giusti, P. A. Macromolecules 1991, 24, 2253.
29. Yamada, K.; Matsumoto, S.; Tagashira, K.; Hikosaka, M. Polymer 1998, 39, 5327.
30. Zuiderduin W. C. J.; Westzaan, C.; Huetink, J.; Gaymans, R. J. Polymer 2002, 44, 261.
31. Thio, Y. S.; Argon, A. S.; Cohen, R. E.; Weinberg, M. Polymer 2002, 43, 3661.
32. Elmajdoubi, M.; Vu-Khanh, T. Theor Appl Fract Mech 2003, 39, 117.
33. Galeski, A. Prog Polym Sci 2003, 28, 1643.
34. Galeski A.; Argon A. S.; Cohen R. E. Macromolecules 1989, 21, 2761.
35. Castagnet, S.; Deburck, Y. Mater Sci Eng A 2007, 448, 56.
36. Pawlak, A.; Galeski, A. Macromolecules 2005, 38, 9688.
37. Pawlak, A.; Galeski, A. Macromolecules 2008, 41, 2839.
38. Kim, G. M.; Michler, G. H. Polymer 1998, 39, 5689.
39. Kim, G. M.; Michler, G. H.; Gahleitner, M.; Fiebig, J. J Appl Polym Sci 1996, 60, 1391.
40. Tjong, S. C. Mater Sci Eng R 2006, 53, 73.
41. Lin, Y.; Chen, H.; Chan, C.-M.; Wu, J. S. Eur Polymer J 2011, 47, 294.
42. Ravi, S.; Takahashi, K. Polym Eng Sci 2002, 42, 2146.